Journal of Materials Chemistry A

ROYAL SOCIETY OF CHEMISTRY

PAPER

View Article Online
View Journal | View Issue



Cite this: J. Mater. Chem. A, 2021, 9, 15355

# Dendrite suppression by anode polishing in zinc-ion batteries†

Zhenyu Zhang, [ab] Samia Said, [a] Keenan Smith,[a] Ye Shui Zhang, [ab] Guanjie He, [acd] Rhodri Jervis, [ab] Paul R. Shearing, [ab] Thomas S. Miller *[ab] and Dan J. L. Brett *[ab]

Received 31st March 2021
Accepted 23rd June 2021

DOI: 10.1039/d1ta02682h

rsc.li/materials-a

Aqueous zinc-ion batteries (ZIB) with Zn metal anodes are promising candidates for future electrochemical energy storage devices. However, Zn dendrite growth greatly limits their practical application. Many recent studies have developed methods to hinder dendrite formation and growth, including interfacial barrier layers, alternative anode and cathode materials, new electrolyte chemistries, or complex structured separators. However, relatively little attention has been paid to the structure of the Zn foil itself. Herein, by simply polishing the Zn foil before electrochemical operation, the morphological uniformity and reversibility of the deposited Zn layer on the metal anode is significantly improved during cycling, compared to that of as-received Zn foils. By combining *ex situ* optical microscopy (OM) and *in situ* electrochemical atomic force microscopy (EC-AFM), it is demonstrated that the initial roughness of the Zn foil electrode surface defines the subsequent plating/stripping morphology. The use of flatter foil anodes notably increases ZIB cycle life. This methodology offers a simple and industrially scalable route to wider ZIB utilisation, as well as highlighting an important consideration for future battery research.



## Introduction

Although lithium-ion batteries (LIBs) have been a dominant technology in the energy storage market for decades, concerns around their safety, cost and environmental impact mean there is an active search for potential alternatives.[1] Among the candidates for future inexpensive, safe and environmentally benign batteries, rechargeable zinc-ion batteries (ZIBs) have received extensive attention owing to their compatibility with aqueous electrolytes, high theoretical capacity (820 mA h $g^{-1}$), low redox potential (−0.76 V *vs.* the standard hydrogen electrode) and low cost.[2,3] Effective ZIBs have been produced by combining various metal oxide cathodes and mild aqueous electrolytes, which have much higher ionic conductivities than organic electrolytes (~0.1 S $cm^{-1}$ *vs.* ~1–10 mS $cm^{-1}$), with a metallic Zn foil anode.[4] However, state-of-the-art ZIBs are still far from satisfactory for widespread application due to their low coulombic efficiency (CE) and short cycle life.[5]

Metallic anodes offer very high energy densities in batteries due to the exclusion of all active material support/encapsulation structures, conductive additives, binders and current collectors.[6] However, dendrite nucleation and growth upon these foils (*e.g.* $Li^+$, $Na^+$, $K^+$, $Ca^{2+}$, $Al^{3+}$) can lead to active material loss (isolation) or internal short circuit, leading to cell degradation and potentially catastrophic failure.[7] During Zn deposition on the metal anode surface, $Zn^{2+}$ ions are reduced to initially form random protuberances by overcoming the energy barrier (nucleation over-potential). Further deposition at these nucleation sites is then preferential, in part due to a strengthened local electric field, leading to the growth of dendrites.[8] These structures easily penetrate the separator between electrodes, due to the high Young's modulus of Zn (~108 GPa, *vs.* ~5 GPa for Li).[9] Many factors influence the nucleation and growth of Zn dendrites, such as substrate material and structure, ion concentration and mobility, electric field distribution, electrochemical operation conditions, electrolyte pH and temperature.[10] In particular, it has been reported that the electrolyte composition and the current density at the electrode are major influencers of dendrite morphology,[11] which can vary from a 1D ramified cone-like topology, to 2D hexagonal platelets and dense 3D structures.[12]

Common strategies to achieve uniform Zn deposition include (1) introducing a protection layer on the electrode surface to help homogeneously distribute ions and the electric field;[13,14] (2) optimizing the material and structure of the Zn-containing electrode, promoting charge transfer;[15,16] (3)

[a]Electrochemical Innovation Lab, Department of Chemical Engineering, University College London, Torrington Place, London, WC1E 7JE, UK. E-mail: t.miller@ucl.ac.uk; d.brett@ucl.ac.uk

[b]The Faraday Institution, Quad One, Becquerel Avenue, Harwell Campus, OX11 ORA, UK

[c]Department of Chemistry, University College London, London WC1H 0AJ, UK

[d]School of Chemistry, University of Lincoln, Lincoln LN6 7DL, UK

† Electronic supplementary information (ESI) available. See DOI: 10.1039/d1ta02682h

modifying the electrolyte, improving interfacial ion migration;[17–19] and (4) designing multifunctional separators.[20] Example solutions using these strategies include (1) interfacial protection of the Zn anode by *in situ* growth of zeolitic imidazolate framework-8 (ZIF-8) layers;[14] (2) design of Zn/carbon nanotube (Zn/CNT) foams[15] or eutectic $Zn_{88}Al_{12}$ (at%) alloys;[16] (3) electrolyte modifying additives[17,18] or use of high concentration electrolytes;[19] and (4) graphene decorated glass fibre separators.[20] All of these solutions, and many others suggested in the literature, would make the commercialisation of ZIBs more difficult by adding additional levels of complexity to both the chemistry and cell design.

An unembellished, as-received Zn foil is still nonetheless the most commonly used anode in ZIB research, due to its simplicity and acceptance as a benchmark.[21] However, the use of these foils as a standard anode relies on the, somewhat unsubstantiated, assumption that Zn foils are consistent in structure and chemistry between suppliers or batches.[22] In fact, the surface properties of as-received Zn foil will vary greatly depending on its preparation method, roughness, presence of surface oxides/carbonates and more.[23] This is a particular problem as it is known that metal electrodeposition is influenced by surface structure.[24] For example, rough surfaces lead to uneven charge distribution and nucleation barriers, leading to the 'tip effect' that can trigger detrimental dendrite formation.[25,26] However, the influence of Zn foil topography on dendrite formation has been little explored. This lack of knowledge may mean that variation in foil morphology may contribute to reported improvements in ZIB performance.

In this work, we show how a simple polishing pre-treatment can greatly increase the plating/stripping cycle life of Zn foil electrodes, significantly improving ZIBs performance. By combining *ex situ* 3D optical microscopy (OM) and *in situ* electrochemical atomic force microscopy (EC-AFM), the early stages of Zn dendrite formation on Zn foils in mild aqueous electrolytes are revealed. The enormous impact of initial foil roughness on the density of Zn nucleation sites, and thus the deposition morphology of Zn, is demonstrated.

## Results and discussion

The long-term electrochemical cycling performance of symmetric coin cells containing Zn foils prepared using different polishing pre-treatments were first evaluated by galvanostatic plating/stripping processes. Fig. 1a presents voltage–time curves of coin cells with as-received Zn foil and Zn foils that had been polished with grinding paper of different 'grit' size (P1200, P2500, P4000), plating/stripping at 1 and −1 mA $cm^{-2}$ for 1 h. The lifetimes, defined as the time until internal short circuit, for the four representative cells shown were 98, 128, 260, and 408 h respectively. The point of internal short circuit is shown by a sharp decrease of voltage hysteresis, as marked by the arrows.[27] The polishing induced a prolonged cycle life before cell failure in all cases, with a clear correlation between cycle life and grinding paper grit size (four times longer for P4000 *vs.* as-received). The cycling performance of another group of the same type of cells confirmed the reliability of the results (Fig. S1,† the cycle lifetimes of these four cells were 64, 110, 305 and 456 h).

In Fig. 1b, the enlarged voltage–time curve during the first plating/stripping cycle of each cell is plotted. The Zn nucleation over-potential (the bottom of the voltage curve) and plating over-potential (the plateau voltage) are used to evaluate the energy barrier of electrochemical Zn nucleation and deposition, respectively.[28] For the as-received Zn, and those polished with P1200, P2500, and P4000, the nucleation over-potentials were close to −0.24, −0.14, −0.13, and −0.13 V respectively, with corresponding plating over-potentials of −0.10, −0.06, −0.04, and −0.03 V. Although the variation in over-potential is small between the polished samples, all offer significant improvement over the as-received Zn, indicating improved nucleation and deposition dynamics, and higher energy efficiency.[29] Equivalent first plating/stripping cycle voltage–time curves of the four samples were also obtained in electrochemical cells during *in situ* EC-AFM experiments (Fig. S2†), showing consistent results. After 1 h of stripping, the potential of the as-received Zn foil electrode rose slightly (from 0.06 to 0.12 V), which is more than for other electrodes. This increase of potential indicates an increase of the internal resistance of the cell as the current density is constant, which is attributed to the stripping of bulk Zn rather than plated Zn.[30] In contrast, the P4000 polished Zn foil cell possessed the lowest stripping potential, representing the best Zn plating/striping reversibility. During the whole cycling life, the P4000 polished Zn foil maintained the lowest voltage range, while the as-received Zn foil has the largest, revealing the former has more favourable Zn deposition/dissolution kinetics. Fig. 1c shows that the cell with the P4000 polished Zn still had the smallest potential rise during plating/stripping after 50–54 h.

It has been reported that a dense and thin $Zn_5(CO_3)_2(OH)_6$ passivation layer is spontaneously formed on the surface of Zn foils when they are exposed to air due to the oxidation by oxygen and moisture. Although this layer is difficult to detect, its removal has been demonstrated to reduce the energy barrier for Zn plating/stripping and improve cycle life.[31] The removal of this layer may explain the lowered over-potential of the polished Zn foil electrodes, compared to the as-received Zn foil. It's removal may also prolong cycle life.

As a ZIB cycles it has been reported that in alkaline electrolytes an insoluble ZnO layer is formed during discharge, which causes a charge transfer barrier for subsequent reactions,[32] whereas in mild aqueous electrolytes no ZnO layer forms and $Zn^{2+}$ ions can be reversibly stripped from/plated onto the surface of a Zn metal electrode. To eliminate the possibility that there is a charge-transfer inhibiting ZnO layer on the surface of the as-received Zn foil, XRD was carried out. As shown in Fig. S3,† no ZnO peaks were detected.[33] It has also been shown that a side reaction can form a thin $Zn_4SO_4(OH)_6 \cdot xH_2O$ layer on the electrode surface during cycling.[34,35] As the cells with as-received and P1200 polished Zn foil electrodes have higher and more unstable plating/stripping potentials, they may be suffering more severely from this side reaction than the P2500 and P4000 cells. However, overall improvement in cell behaviour after polishing can primarily be attributed to a reduction in

 

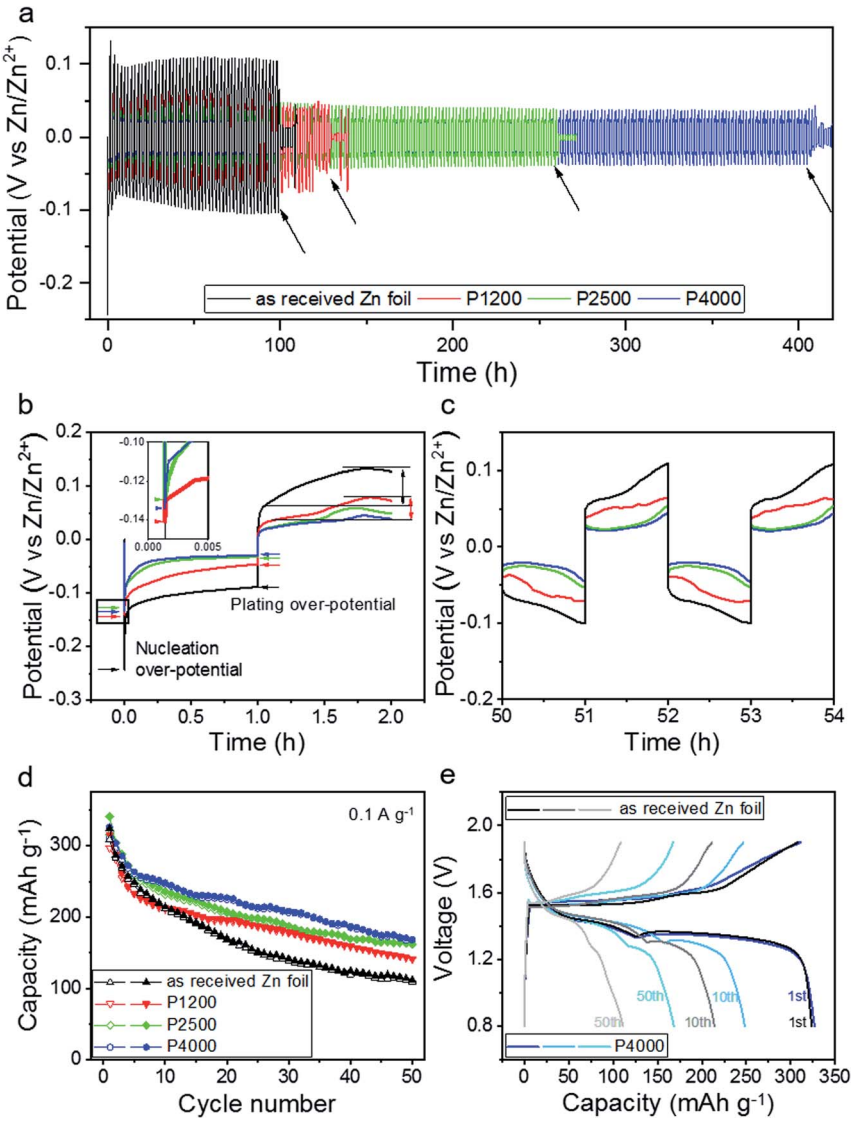


Fig. 1 (a) Electrochemical plating/stripping cycles of symmetric coin cells with the four Zn foil electrodes (as-received, polished with P1200, P2500, P4000 grind paper), with current density of ±1 mA $cm^{-2}$ for 1 h at room temperature. (b) The potential profiles of the four coin cells during the first plating and stripping cycle. The nucleation over-potential in the square area is enlarged in the inset. (c) The potential profiles of the four coin cells after 50–54 h of cycling. (d) Cycling performance of full cells with the four Zn anodes *vs.* a sodium pre-intercalated $Na_{0.65}Mn_2O_4 \cdot 1.31H_2O$ cathode. Galvanostatic charge/discharge at a current density of 0.1 A $g^{-1}$. Solid symbols show the discharge capacity, empty symbols show the charge. (e) Charge/discharge profiles of full cells with as-received Zn foil and P4000 polished Zn foil anodes, for their 1st, 10th and 50th cycles.

the number of sites for dendrite nucleation/growth and a more consistent flux across the surface. The smoother surface of the electrode will also induce a more homogeneous electric field distribution at the electrode/electrolyte interface, promoting even nucleation and growth of plating/stripping Zn layer during cycling.

Although it is interesting to understand the impact of polishing in symmetrical (Zn/Zn cells), it is important to also investigate if any improvement translates into full asymmetric cells. Here full ZIB cells were assembled by coupling the four Zn foil electrodes with a $Na^+$ pre-intercalated δ-$Na_{0.65}Mn_2O_4 \cdot 1.31H_2O$ cathode in the 3 M $ZnSO_4$ electrolyte.[36] The cells were discharge/charge cycled at a constant current of 0.1 A $g^{-1}$, between 0.8 and 1.9 V. As shown in Fig. 1d, the specific capacity of all four cells for the first charge was between 300 and 315 mAh $g^{-1}$. However, the cells with polished Zn foil electrodes show significantly improved capacity retention compared to the as-received Zn foil. Fig. 1e presents the charge/discharge profiles for the full cells with as-received Zn foil and P4000 polished Zn foil anodes for their 1st, 10th and 50th cycles, respectively. They exhibit similar discharge plateaus during the first discharge (the plateau at ~1.4 V is attributed to $H^+$ insertion and the one at ~1.2 V $Zn^{2+}$ insertion),[36] but lower capacity contributions from both $H^+$ and $Zn^{2+}$ insertion regions are observed for the full cell with the as-received Zn foil anode, when compared to the P4000 Zn foil, after 10 and 50 cycles. This

shows that polishing the Zn foil also improves the cycling performance of full cells, due to reduced roughness.[31]

To explore the mechanisms driving the notable improvement in plating/stripping performance after polishing, *ex situ* 3D OM and *in situ* EC-AFM of the symmetric electrochemical cells with different Zn foil electrodes were conducted. The initial, pre-cycling, morphology of the four Zn foil surfaces are presented in 4000 times magnified OM images in Fig. S4.† The surface morphology of the as-received Zn foil shows alternative lines of peaks and trenches, with a height difference of ± >1 μm. The flatness of the surface is improved by polishing, with finer grit grinding paper reducing roughness (increasing flatness) as shown by the roughness value (arithmetic mean height, Sa) obtained from the 3D OM images; the Sa for as-received, P1200, P2500 an P4000 Zn foils were 0.4 (±0.05), 0.2 (±0.03), 0.16 (±0.01), 0.13 (±0.01) μm, respectively. AFM images (Fig. S4,† 50 × 50 μm, collected in air) indicate a similar order of magnitude roughness for the Zn foils, resulting in Ra (arithmetical mean deviation) values of 227, 189, 20.6, 19.4 nm for as-received, P1200, P2500 and P4000 polished Zn foils, respectively.

Fig. 2 displays the OM images (with corresponding 3D maps below) of the as-received Fig. 2(a–d) and P4000 polished Fig. 2(e–h) Zn foils, comparing the initial morphology Fig. 2(a and e) with that after plating for 1 min Fig. 2(b and f), 1 h Fig. 2(c and g) and stripping for 1 h Fig. 2(d and h). The surface of the polished Zn foil can be seen to be visibly smoother than that of as-received Zn foil, even after plating for 1 min, with smaller and more homogeneous nucleation sites. Despite the small curvature in the foil, the maximum height of the polished foil shown in Fig. 2f is only 1.9 μm, while in Fig. 2b, which shows the equivalent data for as-received Zn, bulk Zn crystallites can be seen to already be present, with a maximum height of 4.7 μm. The areas within the white rectangular boxes in Fig. 2b and f are enlarged in Fig. S5,† highlighting the roughness. The Sa values from these areas were calculated to be 0.69 and 0.11 μm, and the nucleated crystals are estimated to be between 1–10 μm and 0.1–1 μm for the as-received and P4000 Zn foils respectively. The nucleation sites for the as-received foil tended to be along the peak lines, rather than the trench areas, ascribed to a locally enhanced electrical field strength.[37]

After plating for 1 h, the maximum height of the individual crystals in Fig. 2c grows to 39.2 μm due to the accumulating deposition at the top of existing Zn particles. By contrast, the maximum height of the P4000 polished Zn foil only reaches 10.7 μm, despite the same degree of charge transfer, as a more layer-like structure of much smaller Zn particle forms. The Sa for Fig. 2c and g are 7.1 and 1.2 μm, indicating a significant difference in Zn deposition behaviour for the as-received and polished Zn foil. After 1 h of stripping, the maximum height of the two samples decreases by ~30% (from 39.2 to 27.4 μm for as-received, Fig. 2d) and ~50% (from 10.7 to 5.0 μm for polished, Fig. 2h), with Sa values of 4.48 μm and 0.24 μm, respectively. Although the flatness of the P4000 polished Zn foil isn't completely recoverable after stripping (ideally only the Zn

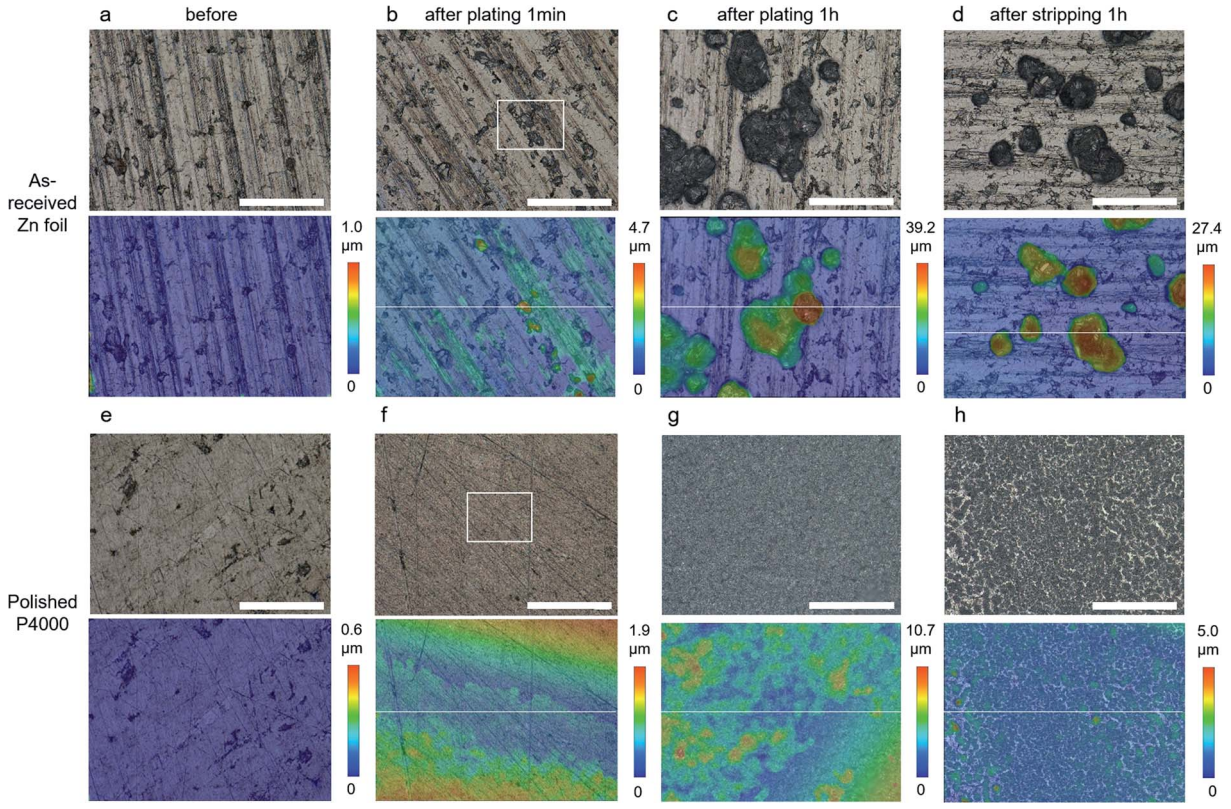


Fig. 2 OM images (1000 times magnification, with 3D colour images below) of as-received (a–d) and P4000 polished (e–h) Zn foil electrodes before plating (a and e), after plating for 1 min (b and f) and 1 h (c and g), and after stripping for 1 h (d and h). Scale bars are 100 μm.

 

deposited would be removed, not changing the initial Zn substrate), the plating/stripping uniformity of the Zn foil electrode is significantly improved by the polishing treatment, explaining the significant improvement in cycling stability for these Zn electrodes.

Fig. S6† presents the *ex situ* OM images (with 3D colour plots) of all four samples at the different stages of the electrochemical process discussed above, *i.e.* before operation, after plating for 1 min, 10 min, 1 h and stripping for 1 h, at 1000 times magnification. All of the polished Zn electrodes offer a much-improved uniformity of Zn deposition, showing finer structures both after plating and stripping. There is a clear correlation between the initial roughness of Zn electrodes and the resulting deposited Zn structure; the Zn layers after plating and stripping are more uniform and thinner at smoother electrodes, indicating a better ability to suppress dendrite growth.

For a more in-depth comparison of the Zn structures, height profiles along the white lines shown in Fig. 2b–d and f–h are plotted in Fig. 3a and b, respectively. The positions of the white lines were selected because they represent a typical morphology for the corresponding Zn foils. The same position could not easily be compared due to the *ex situ* nature of these experiments. For the as-received Zn foil electrode, the height of the deposited crystals rises quickly during plating and then retracts somewhat during stripping, leaving protruding Zn particles. In comparison, for the P4000 polished Zn foil electrode, the height of the deposited layer increased evenly up to only 5 μm across the surface during plating, and this additional layer is almost reversibly removed to a relatively smooth surface during striping. Similarly, the height profiles (along the white lines shown in Fig. S6†) of the four Zn samples at different stages of plating and stripping are shown in Fig. S7,† which reveals the significantly improved height uniformity during plating/stripping that has been enabled by the polishing treatment. Fig. 3c shows the roughness (Sa) values during the plating/stripping procedure of the four samples, obtained from the 1000 times magnification images. The Sa value of the as-received Zn foil increases from 0.4 μm to 11.02 μm after plating for 1 h (27.5 times that of the initial foil), and then maintains a value of 5.76 μm (14.4 times that of the initial foil) after stripping. Comparatively, it increases from 0.13 μm to 1.37 μm (10.5 times that of the initial foil) and decreases to 0.48 μm (only 3.7 times that of the initial foil) for the P4000 polished Zn foil.

To further investigate the improved Zn deposition morphology *in situ* EC-AFM measurements (Fig. S8†) were conducted using a similar plating/stripping procedure as discussed above. Fig. S9† presents the as-received Zn foil morphology during the first 2 cycles of a repeated plating/stripping test. During plating, some small particles (~1 μm diameter) appeared on the surface of the Zn foil, which are likely to be nucleated Zn particles that failed to grow further or induce dendrite formation as they maintained the same size during the process. However, large particles with scale beyond the scan area (50 × 50 $\mu m^2$) and large pits (~7 × 9 $\mu m^2$ area) appeared after the second deposition and second stripping respectively, eventually leading to the failure of AFM image capture. Our previous Zn deposition experiments, with potentiostatic plating at a much lower current density (~0.05 A $cm^{-2}$), suggest that these large particles initially possess a polyhedron structure.[38] It is believed that in the present case (as-received Zn foil, 3 M $ZnSO_4$ aqueous electrolyte, and plating/stripping with a current density of 1 mA $cm^{-2}$), Zn first forms these polyhedron structures (Fig. 2b and S5a†) *via* an epitaxial growth mechanism on Zn surface,[11] before the shape becomes more random, as seen from the OM images in the initial cycles, before finally growing into a fern-like structure during repeated plating/stripping cycles.[18]

Fig. 4 and S10† display the *in situ* EC-AFM images at different stages during the plating procedure for all three polished Zn foil electrodes. Different from that of the as-received Zn foil (Fig. S9†), the morphologies of these foils change immediately once the galvanostatic plating starts. After 1 min plating on the P1200 polished sample, a large number of particles are formed all over the surface (Fig. 4a), with particle size ranging from 0.5 to 5 μm for individual particles and aggregated clusters. It is apparent that the particles are larger at the edges of scratches when compared to those formed at the trench areas. The larger particles grow more quickly, due to the increased flux towards them, and eventually cause EC-AFM image capture to skip lines and fail (after 30 min plating, Fig. S10†). Differently, the P2500 and P4000 polished Zn foils possess much flatter surfaces in the

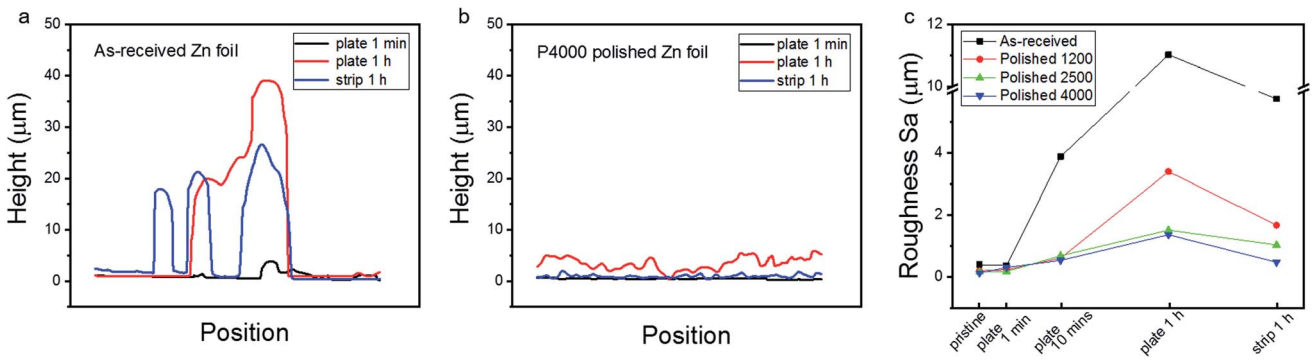


Fig. 3 The height profiles along the white lines in the 3D images of Fig. 1b–d (a) and Fig. 1f–h (b). (c) The roughness Sa values evolution of the four samples during the whole plating/stripping procedure.

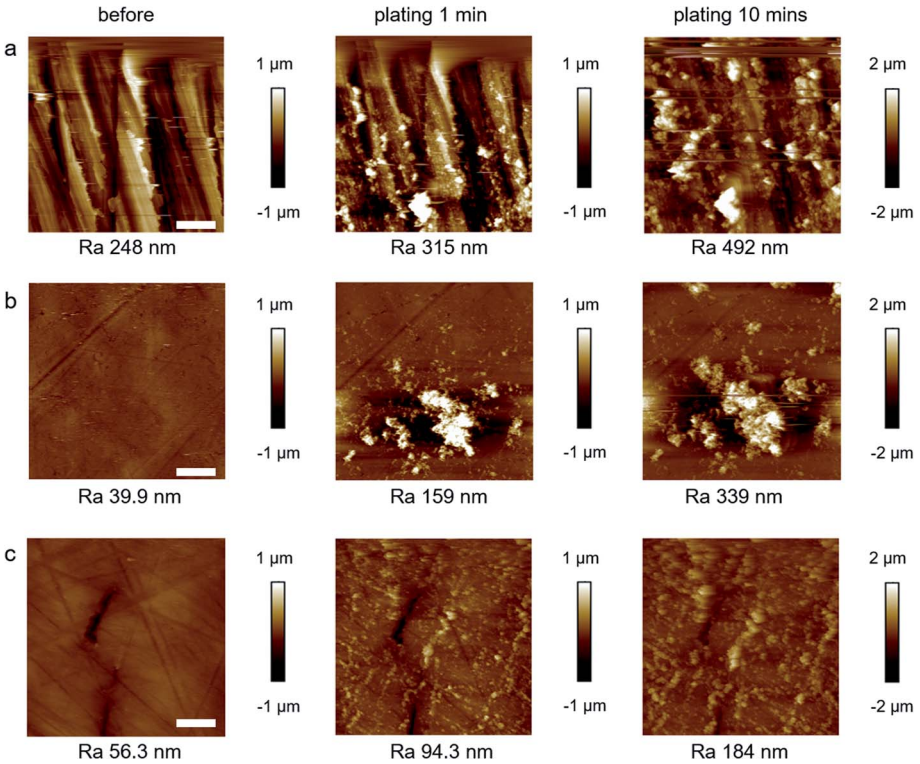


Fig. 4 *In situ* EC-AFM images of polished Zn foil electrodes before and after 1 min and 10 minutes of plating. The Zn foils were polished with (a) P1200, (b) P2500, (c) P4000 grind papers. Scale bars are 10 μm.

early stages of deposition. Although the roughness of the two areas shown does appear similar in these samples, the significantly larger scale images of the same samples collected using the OM shows that the P2500 polished Zn foil is rougher ($0.16 \pm 0.01$ μm) than the P4000 polished Zn ($0.13 \pm 0.01$ μm). The particle size of the deposited Zn after 1 min plating for both samples is smaller (~0.1–1 μm) than that of the P1200 polished Zn electrode. However, the nucleation uniformity between P2500 and P4000 polished Zn foils does show differences after 1 min of plating. For the P2500 sample, the particles randomly gather as large clusters with sizes of up to 10 μm, consistent with observations in the OM experiments, and continue to grow larger and taller in the following plating steps until image capture fails (Fig. S10†). In contrast, small Zn particles are uniformly distributed across the whole surface of the P4000 polished Zn foil without obvious aggregation, although some of the particles are found to be preferentially nucleated at scratch edges. In subsequent plating steps, the particles grow bigger almost homogeneously. Even though some of the particles grow somewhat faster than others, the height is confined within 3 μm after 1 h plating (Fig. S10†), which is in good accordance with the OM images. The roughness (Ra values) after plating for 10 minutes are 492, 339 and 184 nm for the P1200, P2500, and P4000 Zn electrodes, confirming better uniformity of Zn deposition is achieved by finer polishing treatments. Nonetheless, although the P4000 sample does appear to show the lowest post-stripping roughness (Fig. 3c), it should be noted that the variation between this and the P2500 sample is small. There is, however, a major improvement between these samples and the as-received and P1200 polished Zn. The smoother the Zn surface is, the lower the chance of Zn roughening and dendrite formation, supporting the electrochemical evidence.

## Conclusions

We have demonstrated that a very simple and easily industrially applicable anode foil polishing process can dramatically improve the lifetime of ZIBs, far exceeding improvements made using complex chemical and physical processes.[14–20] The electrodes tested showed greatly improved electrochemical plating/stripping stability, when compared to an as-received Zn foil. *Ex situ* OM and *in situ* EC-AFM experiments demonstrated that polished Zn foils with a flattened initial surface induced a uniformly plated/stripped Zn structure, lowering the occurrence of dendrites and short-circuit failure in batteries.

Most importantly, this work has significant implications for both past and future studies on ZIBs with Zn foil anodes. It clearly demonstrates that before materials or methods are reported that improve ZIB stability and lifetime, or comparisons are made to prior works, it is vital that researchers ensure the reported change is, in fact, not simply caused by a difference in initial Zn foil structure.

## Experimental section

### Materials and cells

Zn foils (purity: 99%, thickness: 0.5 mm, Sigma-Aldrich) were both used as-received and polished (manually, circular for 5

 

min) with grinding papers (BUEHLER silicon carbide) of P1200 (average particle size ~15 μm), P2500 (~8.4 μm) and P4000 (~5.0 μm), before being washed with deionized water. The electrolyte contained 3 M $ZnSO_4$ ($ZnSO_4 \cdot 7H_2O$, ACS reagent, 99%, Sigma-Aldrich) in deionized water (PURELAB Option-Q, 18.2 MΩ). The sodium pre-intercalated $Na_{0.65}Mn_2O_4 \cdot 1.31H_2O$ was synthesized by a facile co-precipitation method.[36] The cathode was fabricated by casting the mixed slurry (active material $Na_{0.65}Mn_2O_4 \cdot 1.31H_2O$, polyvinylidene difluoride (PVDF) and super P carbon in the weight ratio of 7 : 1 : 2, in *N*-methyl-2-pyrrolidone (NMP)) onto graphite paper. These electrodes were dried in a vacuum oven for 12 h at 70 °C. The average mass loading for the dried cathodes was 1.5–2.5 mg $cm^{-2}$.

Symmetric coin cells (CR2032) and electrochemical cells for OM and EC-AFM imaging consisted of a Zn working and counter electrode. For the symmetric coin cells Zn foils were cut into circular disks with a diameter of 15 mm and a glass fibre (Whatman glass microfiber filters, grade GF/D) separator was used with the 3 M $ZnSO_4$ electrolyte. The full ZIB coin cells were assembled using the same separator and electrolyte, with a sodium pre-intercalated $Na_{0.65}Mn_2O_4 \cdot 1.31H_2O$ cathode. For the OM cell, two rectangular Zn foils with areas of 1 × 2 $cm^2$ were used as the electrodes in the standard electrolyte, they were connected in parallel with a separation of 2 cm in a beaker. In the EC-AFM cell the electrode area was defined by covering the Zn foil with a Kapton polyimide tape (1 mm thick), with a 1 $cm^2$ hole cut in the centre, before application. The counter electrode was a Ni wire wrapped with Zn foil, which was placed to surround the working electrode in the electrolyte.

### Measurement methods

Symmetric coin cells were tested at a constant temperature of 25 °C (Maccor model 4300 M), by plate/strip cycling at 1 and −1 mA $cm^{-2}$ for 1 h. Full ZIB cells were discharge/charge cycled between 0.8–1.9 V, at a constant current of 0.1 A $g^{-1}$. Both *ex situ* OM and *in situ* EC-AFM experiments were conducted in air with a CHI instruments electrochemical workstation (Model 700E Series Bipotentiostat). A constant current (1 mA $cm^{-2}$) was applied to the Zn working electrode to deposit Zn, before a stripping current (−1 mA $cm^{-2}$) was applied, both for 1 h. *Ex situ* OM (Keyence Digital Microscope VHX-7000) images were obtained after removing the Zn foil from the electrolyte at 1 min, 10 min and 1 h of plating, and 1 h of stripping. 3D images were obtained by a depth composition process, which is achieved by automatically scanning the optical lens throughout the different focal planes. All the roughness values, Sa (arithmetic mean height) by OM or Ra (arithmetical mean deviation) by AFM, were obtained for the the whole area of the images shown by a 3D profile measurement. *In situ* EC-AFM (Bruker Dimension Icon with ScanAsyst) was conducted in contact mode with SNL-10 probes (Bruker), images were captured while the electrochemical process was paused at the time shown in the figures. X-ray diffraction (XRD) was carried out using a StadiP diffractometer from STOE, at a source voltage of 40 kV with a Cu target.

## Conflicts of interest

There are no conflicts to declare.

## Acknowledgements

The present research has been supported by the Faraday Institution (EP/S003053/1), degradation project (FIRG001), LiSTAR project (FIRG014), and EPSRC (EP/R023581/1, EP/P009050/1, EP/N032888/1). TSM thanks the UK EPSRC for support *via* his Fellowship EP/P023851/1. PRS acknowledges The Royal Academy of Engineering (CiET1718/59). GJH acknowledges the EPSRC (EP/V027433/1) and Royal Society (RGS/R1/211080).

## References

1 Y. Liang, H. Dong, D. Aurbach and Y. Yao, *Nat. Energy*, 2020, **5**, 646–656.
2 F. Wan, X. Zhou, Y. Lu, Z. Niu and J. Chen, *ACS Energy Lett.*, 2020, **5**, 3569–3590.
3 Z. Ye, Z. Cao, M. O. L. Chee, P. Dong, P. M. Ajayan, J. Shen and M. Ye, *Energy Storage Mater.*, 2020, **32**, 290–305.
4 Z. Yi, G. Chen, F. Hou, L. Wang and J. Liang, *Adv. Energy Mater.*, 2020, **11**, 2003065.
5 N. Zhang, X. Chen, M. Yu, Z. Niu, F. Cheng and J. Chen, *Chem. Soc. Rev.*, 2020, **49**, 4203–4219.
6 H. Kim, G. Jeong, Y.-U. Kim, J.-H. Kim, C.-M. Park and H.-J. Sohn, *Chem. Soc. Rev.*, 2013, **42**, 9011–9034.
7 B. Lee, E. Paek, D. Mitlin and S.-W. Lee, *Chem. Rev.*, 2019, **119**, 5416–5460.
8 A. Jana, S.-I. Woo, K.-S.-N. Vikrant and R.-E. Garcia, *Energy Environ. Sci.*, 2019, **12**, 3595–3607.
9 J. Zheng, Q. Zhao, T. Tang, J. Yin, C.-D. Quilty, G.-D. Renderos, X. Liu, Y. Deng, L. Wang, D.-C. Bock, C. Jaye, D. Zhang, E. S. Takeuchi, K. J. Takeuchi, A. C. Marschilok and L. A. Archer, *Science*, 2019, **366**, 645–648.
10 J. Hao, X. Li, X. Zeng, D. Li, J. Mao and Z. Guo, *Energy Environ. Sci.*, 2020, **13**, 3917–3949.
11 Q. Yang, G. Liang, Y. Guo, Z. Liu, B. Yan, D. Wang, Z. Huang, X. Li, J. Fan and C. Zhi, *Adv. Mater.*, 2019, **31**, 1903778.
12 L. Ma, M. A. Schroeder, O. Borodin, T. P. Pollard, M.-S. Ding, C. Wang and K. Xu, *Nat. Energy*, 2020, **5**, 743–749.
13 W. Du, E.-H. Ang, Y. Yang, Y. Zhang, M. Ye and C.-C. Li, *Energy Environ. Sci.*, 2020, **13**, 3330–3360.
14 X. Liu, F. Yang, W. Xu, Y. Zeng, J. He and X. Lu, *Adv. Sci.*, 2020, **7**, 2002173.
15 Y. Zhou, X. Wang, X. Shen, Y. Shi, C. Zhu, S. Zeng, H. Xu, P. Cao, Y. Wang, J. Di and Q. Li, *J. Mater. Chem. A*, 2020, **8**, 11719–11727.
16 S.-B. Wang, Q. Ran, R.-Q. Yao, H. Shi, Z. Wen, M. Zhao, X.-Y. Lang and Q. Jiang, *Nat. Commun.*, 2020, **11**, 1634.
17 R. Qin, Y. Wang, M. Zhang, Y. Wang, S. Ding, A. Song, H. Yi, L. Yang, Y. Song, Y. Cui, J. Liu, Z. Wang, S. Li, Q. Zhao and F. Pan, *Nano Energy*, 2021, **80**, 105478.
18 S. J. Banik and R. Akolkar, *Electrochim. Acta*, 2015, **179**, 475–481.

19 F. Wang, O. Borodin, T. Gao, X. Fan, W. Sun, F. Han, A. Faraone, J. A. Dura, K. Xu and C. Wang, *Nat. Mater.*, 2018, **17**, 543–549.
20 C. Li, Z. Sun, T. Yang, L. Yu, N. Wei, Z. Tian, J. Cai, J. Lv, Y. Shao, M. H. Rummeli, J. Sun and Z. Liu, *Adv. Mater.*, 2020, **32**, 2003425.
21 S. Dongmo, D. Stock, J. J. A. Kreissl, M. Groß, S. Weixler, M. Hagen, K. Miyazaki, T. Abe and D. Schröder, *ACS Omega*, 2020, **5**, 626–633.
22 A. Yavas, S. Güler and M. Erol, *J. Aust. Ceram. Soc.*, 2020, **56**, 995–1003.
23 G. Achary and Y. A. Naik, *J. Chem.*, 2013, **2013**, 239747.
24 Y. D. Gamburg, and G. Zangari, Current distribution at rough electrodes, *Theory and Practice of Metal Electrodeposition*, Springer, New York, 2011, ch. 8, pp. 169–170.
25 C. Zhao, X. Wang, C. Shao, G. Li, J. Wang, D. Liu and X. Dong, *Sustainable Energy Fuels*, 2021, **5**, 332–350.
26 J. Becking, A. Gröbmeyer, M. Kolek, U. Bodehorst, S. Schulze, M. Winter, P. Bieker and M. C. Stan, *Adv. Mater. Interfaces*, 2017, **4**, 1700166.
27 Z. Zhao, J. Zhao, Z. Hu, J. Li, J. Li, Y. Zhang, C. Wang and G. Cui, *Energy Environ. Sci.*, 2019, **12**, 1938–1949.
28 S. Wu, Z. Zhang, M. Lan, S. Yang, J. Cheng, J. Cai, J. Shen, Y. Zhu, K. Zhang and W. Zhang, *Adv. Mater.*, 2018, **30**, 1705830.
29 N. Zhang, F. Cheng, Y. Liu, Q. Zhao, K. Lei, C. Chen, X. Liu and J. Chen, *J. Am. Chem. Soc.*, 2016, **138**, 12894–12901.
30 H. Liu, X.-B. Cheng, R. Xu, X.-Q. Zhang, C. Yan, J.-Q. Huang and Q. Zhang, *Adv. Energy Mater.*, 2019, **9**, 1902254.
31 J. Hao, B. Li, X. Li, X. Zeng, S. Zhang, F. Yang, S. Liu, D. Li, C. Wu and Z. Guo, *Adv. Mater.*, 2020, **32**, 2003021.
32 J. Hao, X. Li, X. Zeng, D. Li, J. Mao and Z. Guo, *Energy Environ. Sci.*, 2020, **13**, 3917–3949.
33 H. Yang, L. Chang, L. Wang, D. Yin, D. Wang and Y. Cheng, *Ionics*, 2020, **26**, 3281–3288.
34 J. Hao, X. Li, S. Zhang, F. Yang, X. Zeng, S. Zhang, G. Bo, C. Wang and Z. Guo, *Adv. Funct. Mater.*, 2020, **30**, 2001263.
35 X. Zhou, Y. Lu, Q. Zhang, L. Miao, K. Zhang, Z. Yan, F. Li and J. Chen, *ACS Appl. Mater. Interfaces*, 2020, **12**, 55476–55482.
36 H. Dong, J. Li, S. Zhao, Y. Jiao, J. Chen, Y. Tan, D. J. L. Brett, G. He and I. P. Parkin, *ACS Appl. Mater. Interfaces*, 2021, **13**, 745–754.
37 X. Guan, A. Wang, S. Liu, G. Li, F. Liang, Y.-W. Yang, X. Liu and J. Luo, *Small*, 2018, **14**, 1801423.
38 X. Guo, Z. Zhang, J. Li, N. Luo, G.-L. Chai, T. S. Miller, F. Lai, P. Shearing, D. J. L. Brett, D. Han, Z. Weng, G. He and I. P. Parkin, *ACS Energy Lett.*, 2021, **6**, 395–403.